Matthias Fuchs Publications   Research Papers in Physics and Astronomy

2015

Anomalous nonlinear X-ray Compton scattering

Matthias Fuchs
University of Nebraska-Lincoln, mfuchs@unl.edu

Mariano Trigo
SLAC National Accelerator Laboratory, mtrigo@slac.stanford.edu

Jian Chen
SLAC National Accelerator Laboratory, chenjian@slac.stanford.edu

Shambhu Ghimire
SLAC National Accelerator Laboratory, shambhu@slac.stanford.edu

Sharon Shwartz
Bar Ilan University, Sharon.shwartz@biu.ac.il

See next page for additional authors

Authors

Matthias Fuchs, Mariano Trigo, Jian Chen, Shambhu Ghimire, Sharon Shwartz, Michael Kozina, Mason Jiang, Thomas Henighan, Crystal Bray, Georges Ndabashimiye, Philip H. Bucksbaum, Yiping Feng, Sven Herrmann, Gabriella A. Carini, Jack Pines, Philip Hart, Christopher Kenney, Serge Guillet, Sébastien Boutet, Garth J. Williams, Marc Messerschmidt, M. Marvin Seibert, Stefan Moeller, Jerome B. Hastings, and David A. Reis

UNIVERSITY OF Nebraska Lincoln

digitalcommons.unl.edu

Anomalous nonlinear X-ray Compton scattering

Matthias Fuchs,[1,2] Mariano Trigo,[2,3] Jian Chen,[2,3] Shambhu Ghimire,[2] Sharon Shwartz,[4]

Michael Kozina,[2,3] Mason Jiang,[2,3] Thomas Henighan,[2,3] Crystal Bray,[2,3] Georges Ndabashimiye,[2]

Philip H. Bucksbaum,[2] Yiping Feng,[5] Sven Herrmann,[6] Gabriella A. Carini,[6] Jack Pines,[6] Philip Hart,[6]

Christopher Kenney,[6] Serge Guillet,[5] Sébastien Boutet,[5] Garth J. Williams,[5] Marc Messerschmidt,[5,7]

M. Marvin Seibert,[5] Stefan Moeller,[5] Jerome B. Hastings,[5] and David A. Reis[2,3]

1 Department of Physics and Astronomy, University of Nebraska-Lincoln, Lincoln, Nebraska 68588, USA.
2 Stanford PULSE Institute, SLAC National Accelerator Laboratory, Menlo Park, California 94025, USA.
3 Stanford Institute for Materials and Energy Sciences, SLAC National Accelerator Laboratory, Menlo Park, California 94025, USA.
4 Department of Physics, Institute for Nanotechnology and Advanced Materials, Bar Ilan University, Ramat Gan 5290002, Israel.
5 Linac Coherent Light Source, SLAC National Accelerator Laboratory, 2575 Sand Hill Road, Menlo Park, California 94025, USA.
6 SLAC National Accelerator Laboratory, Menlo Park, California 94025, USA.
7 BioXFEL NSF Science and Technology Center, 700 Ellicott Str., Buffalo, New York 14203, USA.

Corresponding author — M. Fuchs, email mfuchs@unl.edu

Abstract
X-ray scattering is typically used as a weak linear atomic-scale probe of matter. At high intensities, such as produced at free-electron lasers, nonlinearities can become important, and the probe may no longer be considered weak. Here we report the observation of one of the most fundamental nonlinear X-ray–matter interactions: the concerted nonlinear Compton scattering of two identical hard X-ray photons producing a single higher-energy photon. The X-ray intensity reached $4 \times 10^{20}\,\mathrm{W\,cm^{-2}}$, corresponding to an electric field well above the atomic unit of strength and within almost four orders of magnitude of the quantum-electrodynamic critical field. We measure a signal from solid beryllium that scales quadratically in intensity, consistent with simultaneous non-resonant two-photon scattering from nearly-free electrons. The high-energy photons show an anomalously large redshift that is incompatible with a free-electron approximation for the ground-state electron distribution, suggesting an enhanced nonlinearity for scattering at large momentum transfer.

X-ray scattering is primarily sensitive to the spatial position of electrons and their momentum distribution.[1, 2] Elastic X-ray scattering forms the basis of atomic-scale structural determination,[3] whereas inelastic Compton scattering[4] is often used as a spectroscopic probe of both single-particle excitations and collective modes.[5] Linear Compton scattering from weakly bound electrons (that is, when the inelastic energy transfer is large compared to the relevant binding energies) is described well by the impulse approximation (IA), which treats the electrons as quasi-free.[6] In this limit, the spectrum of the Compton-scattered photons at a given momentum transfer is a direct probe of a material's ground-state momentum distribution.

At high intensities, such as those generated by X-ray free-electron lasers (XFELs), nonlinear X-ray–matter interactions can become important.[7–16] For elastic X-ray scattering in crystals the second-order nonlinearity has been considered theoretically as originating from the classical anharmonic motion of a periodic collection of nearly-free electrons in a strong field.[17,18] For free electrons, nonlinear scattering was described semiclassically within the framework of quantum electrodynamics (QED) by Brown and Kibble half a century ago.[19] The dynamics of the interaction and the scattering rate depend strongly on the Lorentz-invariant quantity $\eta = eE/(m_e c \omega)$. This dimensionless field-strength parameter represents the root-mean-square (r.m.s.) transverse momentum (normalized to $m_e c$) imparted to the electron by a classical electromagnetic wave of r.m.s. field strength E and angular frequency ω; here e is the elementary charge, m_e the electron rest mass and c the speed of light.

Previous experiments have investigated the interactions of electrons with high-intensity ($\sim 10^{18}\,\mathrm{W\,cm^{-2}}$) optical radiation in the relativistic regime, $\eta \sim 1$ (that is, when the velocity of the electron quivering in the field becomes relativistic). They include the generation of harmonics from plasma electrons[20] and multiphoton Compton scattering from a beam of ultrarelativistic free electrons in a near head-on collision geometry.[21]

To approach this relativistic regime with hard X-rays requires intensities of $\sim 10^{26}\,\mathrm{W\,cm^{-2}}$, well beyond what is at present achievable. Nonetheless, concerted two-photon scattering processes can be observable from solid targets at orders of magnitude less intensity, on the basis of perturbative scaling. For $\eta < 1$, a free electron will undergo anharmonic motion with the nth harmonic contribution to the induced current $j_{n\omega} \sim \eta^{(n-1)} j_\omega$, and thus the cross-section for nonlinear scattering will scale as $\sigma^{(n)} \sim \eta^{2n-2} r_0^2$, where r_0 is the classical electron radius. Models that treat the solid as a collection of free electrons have been successful in describing perturbative nonlinear X-ray–matter interactions, including non-resonant X-ray second-harmonic generation (XSHG; ref. 16) and the (optically modulated) X-ray susceptibility in X-ray–optical sum frequency generation.[22] The efficiency in the case of (elastic) phase-matched XSHG in diamond was measured to be 6×10^{-11} for peak fields of $\sim 10^{16}\,\mathrm{W\,cm^{-2}}$—in agreement with the free-electron-like model in a periodic medium.[16]

Here we report the observation of anomalous nonlinear X-ray Compton scattering from solid beryllium. We measure the concerted scattering of two hard X-ray photons with energies around 9 keV into a single higher-energy photon red-shifted from the second harmonic. The number of scattered high-energy photons varies quadratically with the FEL intensity, as expected for a second-order nonlinear process, and is well above the measured background. The signal is emitted in a non-dipolar
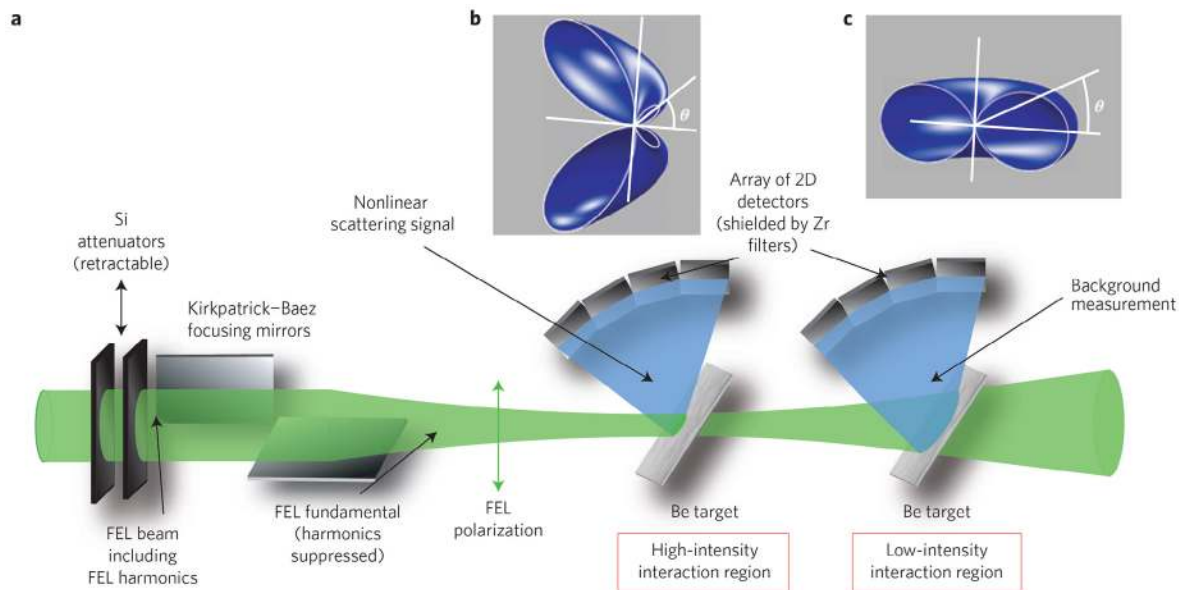
Figure 1. Experimental set-up. a) The XFEL beam with photon energy near 9 keV (green) was incident on two 1-mm-thick Be targets oriented at an incidence angle of 45° located in a He environment. The first target was placed in the ~100 nm XFEL focus (high-intensity interaction region), and a second identical target was placed well out of focus (low-intensity interaction region). This set-up allowed the simultaneous measurement of the signal and background, as the X-rays are transmitted largely unattenuated by the Be. The average pulse energy of the FEL fundamental on the target was varied using Si attenuators. The weaker residual FEL second harmonic and third harmonic (generated in the undulator) were significantly rejected by the focusing mirrors before reaching the target. Scattered radiation from the two interaction regions was collected over a wide solid angle using arrays of four 2D detectors (each detector comprising 140 k pixels covering ~14° × 14° centered at 131°, 117°, 103° and 89° in the polarization plane for the high-intensity arc, which owing to experimental constraints was rotated by −5° relative to the low-intensity arc). During all measurements 250-μm-thick Zr foils were placed directly in front of the detectors. This significantly attenuated the scattered photons near the FEL fundamental while largely transmitting photons with energies just under the Zr K-edge (~18 keV). By varying the incident photon energy from 8.8 to 9.8 keV, the Zr filter acts as an integrating spectrometer for resolving the energy loss in the two-photon Compton signal, $\omega_2'(\omega_0, \theta)$. **b)** Calculated angular distribution of the free-electron nonlinear second-harmonic emission generated by a free electron at rest. In the perturbative regime (normalized vector potential $\eta \sim 2 \times 10^{-3}$), the emission is peaked at a scattering angle of $\theta \sim 130°$ and includes a finite scattering into the FEL polarization direction $\theta = 90°$. **c)** Calculated emission pattern for low-intensity linear scattering (dipole emission), which has a negligible scattering contribution into the polarization direction.

pattern. However, the photon spectrum shows an anomalously large redshift in the nonlinearly generated radiation compared to the free-electron theory and to the simultaneously measured linear scattering from the weak residual FEL second harmonic generated by the undulators.[23] Our observations are incompatible with kinematics for the ground-state electron distribution in the impulse approximation. This additional redshift suggests a novel nonlinear scattering mechanism involving bound-state electrons, despite an X-ray energy of approximately two orders of magnitude above the 1s binding energy.

In our experiments, the maximum intensity was ~4 × 10^{20} W cm^{-2}. This corresponds to a peak electric field of ~5 × 10^{11} V cm^{-1} which is within almost four orders of magnitude of the quantum-electrodynamic critical field,[24,25] yet still well in the perturbative regime ($\eta \sim 2 \times 10^{-3}$). The strong X-ray fields were produced in the ~100 nm focus of the linearly polarized, ~1.5 mJ, 50 fs, Linac Coherent Light Source XFEL, using the Coherent X-ray Imaging (CXI) instrument.[26] The incident X-ray energy was tuned in the range $\hbar\omega_0 = 8.8$–9.75 keV. Two solid Be targets were arranged at a 45° incidence angle (see Figure 1), one at the X-ray focus and the other downstream of the focus where the intensity is low. We chose beryllium because it is a low-Z material with a relatively low photoionization cross-section, favorable ratio of Compton to elastic linear cross-sections[27] and high melting point. The effective target thickness (1.4 mm) is considerably smaller than the linear absorption length of the fundamental (7.3 mm for 9 keV), such that >80% of the beam is transmitted. The angular distribution of the scattered radiation was detected using multiple two-dimensional (2D) pixel array detectors[28] arranged in an arc with radius ~20 cm covering observation angles from 80°–135° in the XFEL polarization plane and approximately ±7° out of

the polarization plane (see Figure 1). The detectors have a coarse intrinsic energy resolution of a few keV, which we use to distinguish between a single (lower-energy) photon near the FEL fundamental and a (higher-energy) photon near the second FEL harmonic. We cannot differentiate between a single higher-energy photon and the pile-up of two lower-energy photons that deposit the same energy into a single pixel during a single shot. To sufficiently reduce the probability of pile-up, we strongly attenuate scattered photons near the fundamental by placing 250-μm-thick Zr foils directly in front of the detectors (see Methods). This highly chromatic filter transmits (~10%) X-rays just under the Zr K-edge ($\hbar\omega_K = 17.996$ keV), while attenuating photons around 9 keV and just above 18 keV each by about seven orders of magnitude (see Methods). Note that owing to the strong chromaticity of the filter coupled with the coarse energy resolution of the detectors, we do not rely on the detectors alone to extract spectral information about the high-energy photons. Instead, we vary the FEL fundamental photon energy and exploit the contrast in the transmission near the Zr absorption edge to discriminate higher-energy photons that have been redshifted by at least $2\hbar\omega_0 - \hbar\omega_K$. The overall background was simultaneously characterized with a nearly identical configuration placed well out of focus, at a significantly lower FEL intensity but with a comparable number of incident photons (see Figure 1). Additional background originates from the linear scattering of the FEL second harmonic that is produced in the undulators.[23] This is substantially reduced before reaching the target by the low reflectivity of the focusing mirrors for photon energies above 11 keV (ref. 26). The scattering of the residual second FEL harmonic was measured to be negligible in comparison to the nonlinear signal; no significant scattered third FEL harmonic was detected.
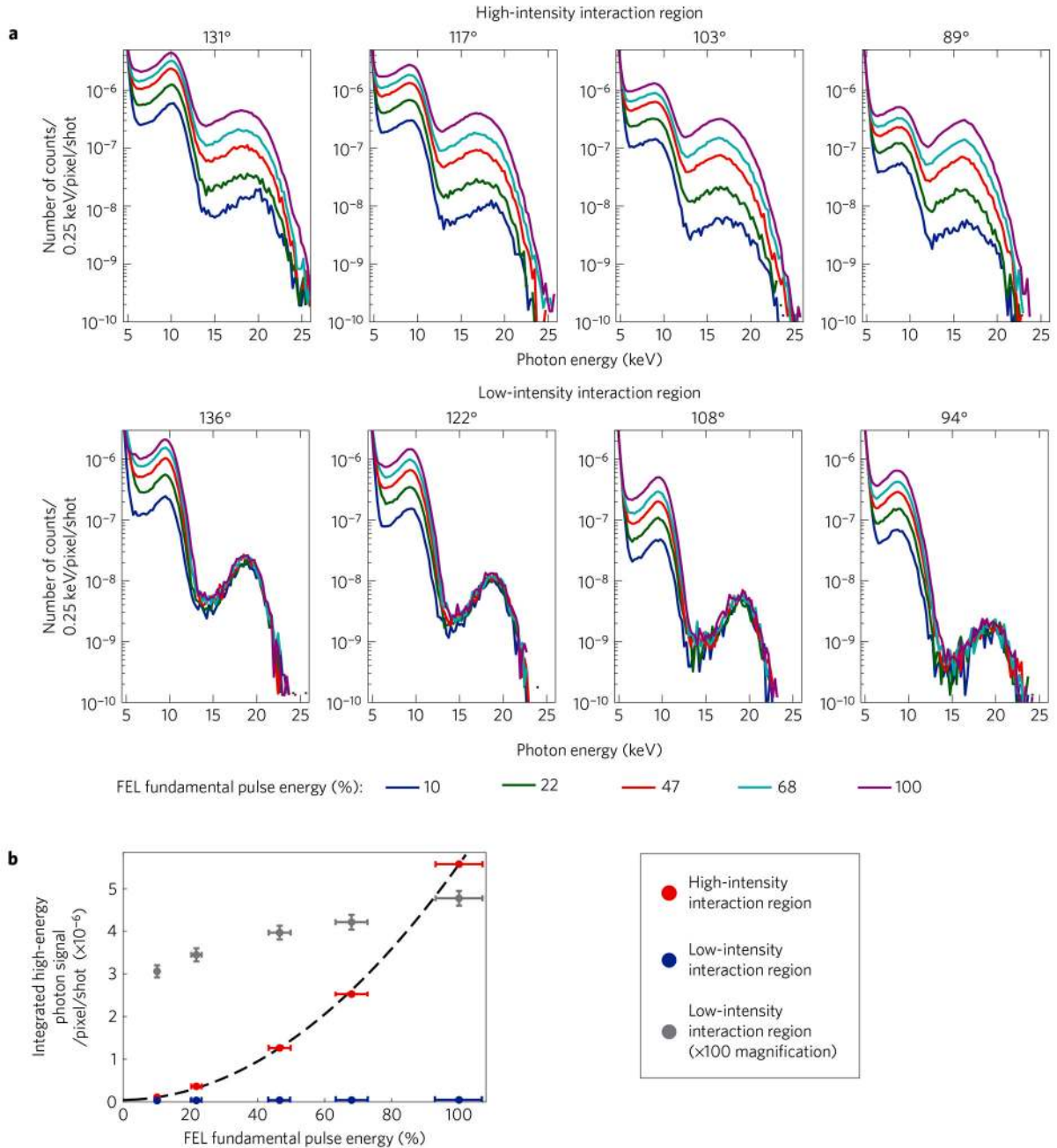
Figure 2. Scattering signal as a function of the FEL fundamental pulse energy and scattering angle. a) Detected signal for FEL fundamental pulse energies ranging from 10 to 100% of the full beam (color coded) at an incident photon energy of 9.25 keV. Each interaction region has four detectors centered at the scattering angle indicated above each plot. The plots show the number of photons per pixel per shot within a 0.25 keV energy bin. The histograms were individually recorded for each FEL pulse and averaged over ~170,000 shots. The detected photons are distributed in peaks near the FEL fundamental and the Zr K-edge (18 keV). The resolution of the detector is limited to a few keV and the energy scale is only approximate, such that the detectors are used solely to distinguish the low- and high-energy photons (see **Methods**). The signal from the high-intensity interaction region (top row) shows a substantial, nonlinear change with the FEL fundamental pulse energy in the higher-energy photon peak, corresponding to $n = 2$ Compton scattering with a redshift of at least 0.5 keV. The peak is substantially broadened compared to the corresponding peak in the low-intensity signal (bottom row) which originates from $n = 1$ Compton scattering of residual FEL second-harmonic photons (18.5 keV) with the same minimum redshift. In addition, near 90° (right column), where the dipole emission pattern of linear scattering is highly suppressed, we measured a significant increase in the high-energy photon signal relative to the low-intensity interaction as well as to the FEL fundamental (at 9.25 keV). The intensity of the FEL fundamental was varied using silicon absorbers before focusing the beam. The effect of the attenuators on the transmission of the residual FEL second harmonic is comparably small (73% at the highest attenuation). Note that the detector signal on any single shot is sparse, and the probability of detecting two photons in a given pixel is negligible. **b)** Integrated high-energy photon signal as a function of the FEL fundamental pulse energy for the detectors near 90°. Red represents the signal originating from the high-intensity interaction, blue from the low-intensity interaction and grey is the low-intensity signal multiplied by a factor of 100 for ease of comparison. The dotted line shows a quadratic fit as a function of FEL intensity for the high-intensity signal, as is expected for a second-order nonlinear perturbative effect. The signal from the low-intensity interaction varies only slightly, consistent with linear scattering of the residual FEL second harmonic and weak attenuation by the Si filters. The horizontal error bars indicate the spread in FEL pulse energy (after post-process filtering) and the vertical error bars indicate one standard deviation from counting statistics, which for the blue and red data points on this scale are smaller than the marker size.
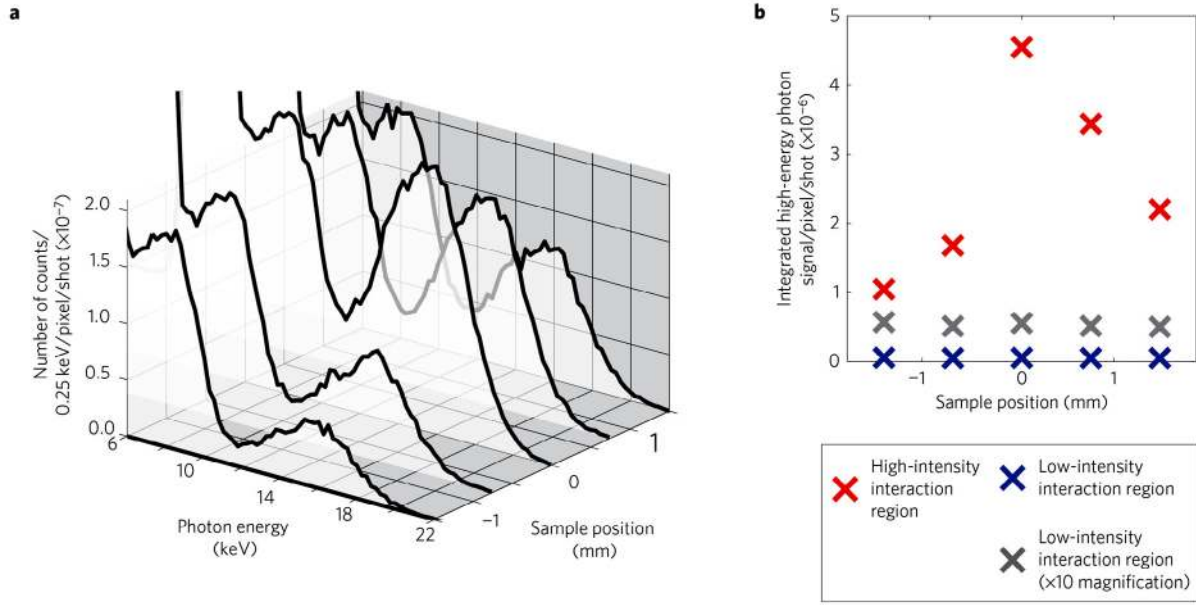
Figure 3. Dependence of nonlinear Compton scattering on sample position relative to the FEL focus. a) Histograms of the detector observing the high-intensity interaction region positioned at an observation angle of 90° for different sample positions with respect to the nominal FEL focal plane. The FEL beam was unattenuated and the fundamental photon energy for this scan was 8.8 keV. Each histogram is averaged over ~60,000 shots. The effective sample length (at 45°) is 1.4 mm. The high-energy photon signal varies strongly with the sample position whereas the ~8.8 keV signal from the high-intensity region and the overall low-intensity signal (over the whole energy range) remain practically constant. Note that the detectors at the other observation angles show a similar behavior. **b)** Integrated high-energy photon signal versus the sample position for the high-intensity interaction (red) compared to the peak at the low-intensity (fixed sample) interaction (blue, grey is multiplied by a factor of 10 for clarity).

We measure the scattered photons as a function of scattering angle and FEL fundamental intensity (Figure 2). The intensity was varied using silicon attenuators placed before the focusing mirrors. For this measurement, the incident photon energy was 9.25 keV, such that the observed higher-energy photons (transmitted through the Zr filter) are redshifted by at least 500 eV from the second harmonic, which is large compared to the 1s binding energy of Be (112 eV). The measured high-energy photon signal from the high-field interaction region shows a significant dependence on the FEL pulse energy (Figure 2a top row) whereas the low-intensity signal is nearly independent of pulse energy (Figure 2a bottom row). In addition there is a substantial high-energy photon signal in the ~90° observation direction for the high-field interaction. The higher-energy photons show a quadratic pulse-energy dependence (Figure 2b) that is consistent with an $n = 2$ second-order perturbative process. For the low-intensity interaction region the signal is nearly independent of the incident FEL fundamental pulse energy, and there is relatively low scattering near 90°. This is consistent with $n = 1$ linear Compton scattering from the residual FEL second harmonic, considering the nearly constant transmission of ~18 keV photons through the Si attenuators. As further evidence of a nonlinear interaction, the $n = 2$ signal shows strong dependence on the positioning of the sample relative to the focal plane, as shown in Figure 3 (measured at the maximum incident pulse energy, and at an incident photon energy of 8.8 keV). The higher-energy photon signal is strongly reduced when the sample is translated on the order of its thickness through the focus, confirming that the dominant nonlinear scattering occurs from the high-intensity region close to the focal plane.

The energy of scattered photons from a single free electron can be deduced through kinematical considerations. Consider the concerted scattering of n photons each with energy ω and momentum $\mathbf{k}$ ($\hbar = c = 1$) from a free electron of initial momentum $\mathbf{p}$, into a single photon (ω_n', $\mathbf{k_n}'$). Energy and momentum conservation lead to the generation of a single photon

with energy

$$\omega_n'(\omega, \theta) = \frac{n\omega + \dfrac{\mathbf{p} \cdot \mathbf{K_n}}{m_e}}{1 + \left(\dfrac{n\omega}{m_e} + \dfrac{\eta^2}{2}\right)(1 - \cos\theta)} \tag{1}$$

where $\mathbf{K_n} = n\mathbf{k} - \mathbf{k_n}'$ is the n-photon momentum transfer and $\cos\theta = \mathbf{k} \cdot \mathbf{k_n}'/(\omega\omega_n')$. For our parameters, ($\eta \sim 2 \times 10^{-3}$), ponderomotive effects are expected to contribute negligibly to the kinematics as the ponderomotive energy, $\eta^2 m_e/2 = 0.6$ eV $\ll \omega_0$. Equation (1) also describes the $n = 1$ linear scattering from bound electrons in the IA. In the IA the bound electrons act as if they had initial momentum $\mathbf{p}$, with an kinetic energy $p^2/(2m_e)$, as opposed to its binding energy, with probability given by the modulus squared of the Fourier transform of its wavefunction.[6]

If the IA were to hold for nonlinear scattering, equation (1) would also be valid for $n > 1$. Thus, for our parameters we would expect the kinematics for n-photon nonlinear scattering for weakly bound electrons to be to a very high degree the same as for the linear ($n = 1$) scattering of a single photon with n times the energy, that is, ω_1' ($\omega = n\omega_0$, θ) (such as from the harmonics produced in the undulator by the FEL process). Nonetheless, nonlinear n-photon processes could be distinguished from the linear case as the rate and angular distribution of nonlinear scattering depend strongly on both the radiation field strength and the order n of the process.[29] As the nonlinear cross-section for free electrons in the perturbative regime scales as $\sigma^{(n)} \sim \eta^{2n-2}$, the scattering signal would scale with the incoming intensity as I^n (quadratically for an $n = 2$ process). In addition, the differential cross-section would show an angular emission distinctly different from that given by the Klein–Nishina formula[30] for linear Compton scattering: for the $n = 2$ perturbative process, the photons scattered from free electrons initially at rest are expected to be emitted in an asymmetric quadrupole-like pattern peaked at an angle of ~130° (in the backward direction, see Figure 1b).[19,29] Importantly, it would have a finite emission
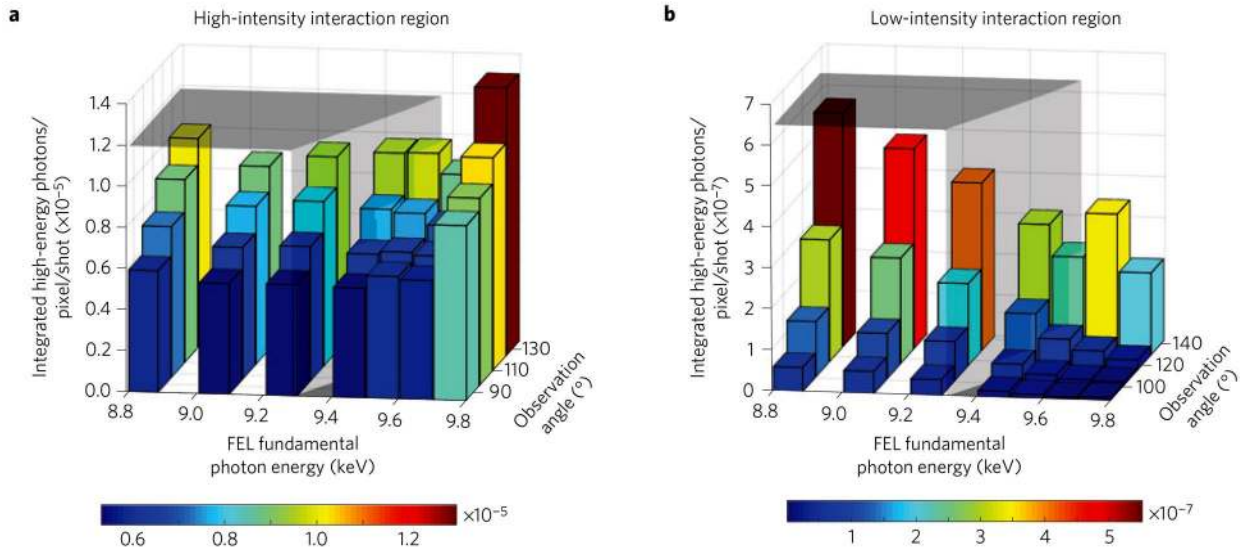
Figure 4. Dependence of the high-energy photon signal on the FEL fundamental photon energy. Angular-resolved signal integrated over the higher-energy photon peak of each detector at 100% FEL transmission for the high-intensity interaction region **(a)** and the low-intensity interaction region **(b)**. The transmission contrast of the 250-μm-thick Zr filters for photons just above ($T = 1 \times 10^{-7}$) compared to just below ($T = 10\%$) the K-edge (at $\hbar\omega_K = 17.996$ keV) was used for a coarse measure of the photon energy loss. The FEL fundamental photon energies range from $\hbar\omega_0 = 8.84$–9.75 keV, corresponding to $2\hbar\omega_0 - \hbar\omega_K = -0.68$ to $+1.5$ keV. The transparent grey curves show the kinematic edges where the scattered photon energy $\hbar\omega' = \hbar\omega_K$ for an electron initially at rest (equation (1) with $p = 0$) for the $n = 2$ nonlinear process in **(a)** and the linear Compton scattering in **(b)** respectively. The low-intensity signals show a cutoff near the kinematic edge that increases with increasing observation angle, which is consistent with equation (1) for $n = 1$ linear Compton of the FEL second harmonic and the finite momentum distribution of the solid in the impulse approximation (IA). There is no corresponding cutoff in the high-intensity scattering signal up to the highest incident photon energy of 9.75 keV. At this photon energy the expected Compton shift in the impulse approximation at 90° is centered around 717 eV (for both $n = 2$ nonlinear scattering of 9.75 keV and linear scattering of 19.5 keV); therefore, the photon energy of the nonlinear signal $\omega_2'(\omega_0, \theta)$ has an anomalous additional redshift of at least 780 eV to be transmitted through the Zr foil. Note that the 9.75 keV signal is averaged only over 30,000 shots, whereas the 8.8 keV and 9.25 keV signals are averaged over 160,000 shots and all other signals over 60,000 shots). The histograms used to generate Figure 4 can be found in the Supplementary Information.

along the FEL polarization (90°) where the linear scattering (dipole emission, Figure 1c) is strongly suppressed.

Although we do not solely rely on the detector for detailed spectral information, the broadening of the nonlinear $n = 2$ signal in Figure 2 suggests that the IA may not hold at high intensity. To further test the IA at high intensity, we vary the incident FEL fundamental photon energy from 8.84 to 9.75 keV and use the Zr K-edge as an integrating spectrometer (see Methods). This allows us sensitivity to scattered photons near the K-edge (that is, those with redshift $\Delta_2 > 2\omega_0 - \omega_K$). If the IA were to hold true, the second-order scattered photon energy ω_2' is centered about ω_K for an incident photon energy of $\omega_0 = 9.28$ (9.59) keV at the minimum (maximum) detection angle of 82° (138°) according to equation (1). The low-intensity signal ($\omega_1'(2\omega_0, \theta) \approx \omega_K$, Figure 4b) shows a strong energy and angle dependence with a cutoff that is consistent with linear Compton scattering of the FEL second harmonic from the loosely bound electrons in Be. However, the nonlinear signal $\omega_2'(\omega_0, \theta)$ at high intensity (Figure 4a) shows no evidence of a cutoff, even up to the highest incident fundamental photon energy of $\omega_0 = 9.75$ keV. This corresponds to a minimum redshift of $\Delta_2 > 1.5$ keV. Note that at $\theta = 90°$ the predicted Compton shift $n = 2$ for the process is centered at ~700 eV in the free-electron limit (equation (1))—thus, there is substantial nonlinear scattering at an additional redshift of at least 800 eV that is absent in the linear signal.

The observation of scattered photons with an additional redshift of this magnitude requires that significant momentum must be exchanged with the medium. The minimum required momentum transfer is comparable to the typical momentum of a 1s electron of Be ($p_{1s} = Z/a_0 = 15$ keV/c, where $a_0 \sim 0.5$ Å is the Bohr radius and $Z = 4$ is the atomic number of Be) but considerably less than the momentum of a primary photoelectron (~100 keV/c). In addition, kinematics rules out non-sequential

processes involving blueshifted single-photon Compton scattering from a primary photoelectron. This suggests either a process with preferential nonlinear scattering from bound electrons, beyond the IA, where the missing momentum is carried in the final state by the recoil of the medium, or nonlinear two-photon scattering from secondary plasma electrons following photoionization within the same FEL pulse.

Figure 4b shows that, in the low-intensity interaction, there is a weak contribution to the scattering for redshifts above the kinematic edge for an electron initially at rest. This is consistent with the bound-state contribution to the linear $n = 1$ Compton scattering background from the FEL second harmonic. Note that the linear Compton profile in beryllium has been measured with extremely high resolution in the momentum transfer out to more than 1.5 atomic units using similar X-ray photon energies.[31] In those studies, details of the conduction band structure as well as a contribution from the 1s core electrons are evident. Importantly, the linear scattering from Be is described well in the free-electron, impulse approximation.

The predominance of the large redshift in the $n = 2$ scattering shown in Figure 4a, however, suggests that any bound-state contribution at high intensity must involve breakdown of the free-electron approximation from the ground-state momentum distribution and a new scattering mechanism. As the Compton redshift is a consequence of energy and momentum conservation, this anomalous redshift indicates that the two-photon scattering cross-section has enhanced contributions from large momentum transfer events, such as those associated with bound electrons.

The interaction term in the light–matter Hamiltonian is given by $H_{int} = (e/m) \mathbf{A} \cdot \mathbf{p} + e^2 \mathbf{A}^2/2m$, where $\mathbf{A}$ is the vector potential operator and $\mathbf{p}$ the electron momentum operator. Diagrams for the leading second-order processes in H_{int} are shown in Figure 5, corresponding to mixed terms in $\mathbf{A} \cdot \mathbf{p}$ and $\mathbf{A}^2$. There are
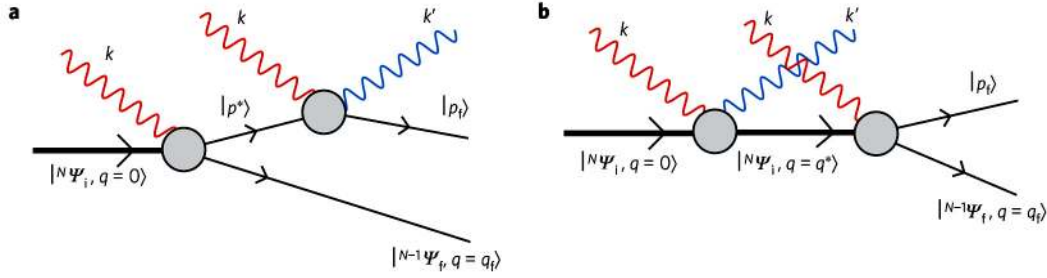
Figure 5. Anomalous two-photon bound-state Compton scattering mechanism. Schematic showing the leading-order diagrams for the concerted scattering of two photons with momentum k (red oscillating line) from N-electron many-body ground state of the medium, $|^N\Psi_i; 0\rangle$ into a higher-energy scattered photon with momentum k' (blue oscillating line), a free electron with momentum p_f and the ($N - 1$)-electron ionized medium with center-of-mass momentum q_f $|^{N-1}\Psi_f; q_f\rangle$. **a**, In this process one photon from the field creates a single intermediate electron in the continuum with momentum $p*$ and the ionized medium. A second photon scatters from the intermediate electron within the intermediate-state lifetime, producing the final-state photon. **b**, In this process a photon from the field first scatters from the N-electron density, producing a higher-energy photon and transferring a portion of the final-state momentum to the medium, but otherwise leaving it in its ground electronic state $|^N\Psi_i; q*\rangle$. The medium then absorbs the second photon within the intermediate-state lifetime, producing the final-state electron and transferring the remaining momentum to the medium. Not shown are diagrams where the intermediate state consists of bound electronic excited states of the medium.

two types of processes leading to the same final state that differ in their intermediate states: an intermediate-state free electron (Figure 5a) and an intermediate scattered photon (Figure 5b). Recently, Hopersky *et al.* have considered theoretically resonant nonlinear sequential processes involving anomalous X-ray scattering from excited atoms where the first photon produces either a real excited atomic state (bound–bound)[32,33] or an excited ion (bound-free).[33] Our results suggest that, even far from resonance, the virtual processes corresponding to the diagrams shown in Figure 5 can be important.

Consider the scattering from a $1s$ electron of a single atom. Inspection of Figure 5 shows that the generalized two-photon double differential cross-section ($d\sigma^{(2)}/d\omega_2'd\Omega$) will scale as a product of single-photon differential cross-sections (photoionization and Compton) and an intermediate-state lifetime. The process in Figure 5a is expected to dominate when the total momentum transfer is similar to the typical $1s$ electron momentum—that is, for low-energy intermediate electron states where the $\mathbf{A}\cdot\mathbf{p}$ matrix element coupling ground and intermediate states is large. The process in Figure 5b will dominate at larger momentum transfers, where the energy difference $\omega_2' - \omega_0$ is small and the intermediate-state lifetime is large. This would lead to a broad spectrum of scattered photons spanning the range of photon energies between the fundamental and near the second harmonic. For scattered photon energies near ω_K (where the filter transmission is maximum), we estimate the total cross-section for the $1s$ electron to be order-of-magnitude comparable to that of a free electron.

Alternatively for the missing momentum to be supplied by an initial hot electron, it needs to have a component of its kinetic energy along $\mathbf{K}_2$, $\hbar^2\mathbf{p}_\parallel^2/2m > 156\,\text{eV}$. Although we cannot completely rule out this process, we note that, for a thermal distribution, this would to lowest order produce a Gaussian broadened, but not shifted spectrum with a half-width at half-maximum of $(2\ln(2)kT/mK_2)^{1/2}$, requiring a plasma temperature $kT > 320\,\text{eV}$ (3.7 $\times$ 10^6 K) to broaden to 18 keV for $\omega = 9.75\,\text{keV}$ and $\theta = 90°$. For comparison we expect $kT \sim 110\,\text{eV}$ at the highest X-ray pulse energies, assuming a photoionization cross-section of 6.9 b atom^{-1} and a fully ionized and thermalized plasma develops within the focal volume during the pulse.

A more complete measurement of the nonlinear Compton-scattered spectrum would allow us to distinguish the relative contributions to the scattering from the nonequilibrium plasma and the bound-state contributions at high intensity. We note that the bound-state processes that we propose should be enhanced near resonance or by phase-matching. If this new

contribution to the inelastic scattering is confirmed it would have implications for measuring structure and dynamics at high intensity in that it represents a previously unconsidered scattering mechanism with the opportunity for combining atomic-scale structural sensitivity with chemical specificity for low-Z atoms.

Methods

X-ray pulses with a photon energy tuned from 8.8 to 9.8 keV and ~0.5% bandwidth (full-width at half-maximum) were focused to a nominally ~100 nm spot using Kirkpatrick–Baez focusing mirrors (depth of focus: ~0.2 mm). The pulses had energies of up to ~1.5 mJ on target and an averaged pulse duration of ~50 fs (envelope), which leads to a focused peak intensity of $4 \times 10^{20}\,\text{W cm}^{-2}$ ($\eta \sim 2 \times 10^{-3}$ for 9 keV). The precise pulse duration and focal size could not be measured. A 1-mm-thick polycrystalline piece of high-purity solid beryllium (Materion PF-60, with >99% beryllium content and a low level of heavy impurities) oriented at an angle of 45° was used as target. Despite the small X-ray cross-sections for scattering and photoionization in Be (attenuation length of 7.3 mm for 9 keV photons[34]), the photon flux is sufficiently high such that the interaction ultimately leads to plasma formation and irreversible damage in a single shot. The sample was stepped to a fresh spot each shot. Scattered photons were detected each shot at 120 Hz using CSPAD 140 K 2D pixel array detectors (PADs; ref. 28) located at observation angles ~80°–135° (see Figure 1). The detectors were substantially shielded from scattering of the FEL fundamental by 250-μm-thick zirconium filters positioned directly in front of the detector (suppression of the 9 keV signal by approximately seven orders of magnitude while transmitting 10% of the signal just below the Zr K-edge at 17.996 keV). We obtain single-photon counting statistics owing to the sparse signal in combination with the 140,000 pixels of each detector. This allowed spatial discrimination of pixels that exceed a particular photon count rate (such as from powder diffraction of the polycrystalline Be). The probability for photon pile-up in the detector at full beam intensity was decreased to ~10^{-8} counts/pixel/shot (three orders of magnitude below the measured signal), by a combination of the Zr filter and post-detection software masking of any pixel that (on average) measured a rate of fundamental photons exceeding 10^{-4} counts/shot. The CSPAD detectors have a coarse energy resolution (few keV), from which the approximate energy deposited by a photon in each pixel could be deduced. We used Cu fluorescence and the scattering signal of the FEL fundamental and second harmonic for a coarse analog-to-digital unit (ADU) to photon energy conversion. For spectral measurements, we use the variation in transmission around the Zr K-edge as an integrating spectrometer. Here, we essentially use the detectors as counters that are capable of separating the high-energy photons from those near the FEL fundamental. In addition, by varying the fundamental photon energy, we are able to discriminate higher-energy photons with a minimum energy loss relative to twice the fundamental. The harmonic content in the FEL beam (generated in the undulator) at hard X-ray energies is <0.1% (second harmonic) and <2% (third harmonic) compared to the fundamental power.[35] The FEL harmonics were suppressed before reaching the sample

References

1. James, R.W. *The Optical Principles of the Diffraction of X-rays* (Ox Bow Press, 1982).

2. Warren, B. E. *X-ray Diffraction* (Addison-Wesley, 1969).

3. Ladd, M. F. C. & Palmer, R. A. *Structure Determination by X-ray Crystallography* (Springer, 2003).

4. Compton, H. The spectrum of scattered X-rays. *Phys. Rev.* **22,** 409–413 (1923).

5. Platzman, P. M. & Tzoar, N. X-ray scattering from an electron gas. *Phys. Rev.* **139,** 410–413 (1965).

6. Eisenberger, P. & Platzman, P. M. Compton scattering of X rays from bound electrons. *Phys. Rev. A* **2,** 415–423 (1970).

7. Young, L. et al. Femtosecond electronic response of atoms to ultra-intense X-rays. *Nature* **466,** 56–61 (2010).

8. Doumy, G. et al. Nonlinear atomic response to intense ultrashort X rays. *Phys. Rev. Lett.* **106,** 083002 (2011).

9. Hoener, M. et al. Ultraintense X-ray induced ionization, dissociation, and frustrated absorption in molecular nitrogen. *Phys. Rev. Lett.* **104,** 253002 (2010).

10. Fang, L. et al. Double core-hole production in N_2: Beating the Auger clock. *Phys. Rev. Lett.* **105,** 083005 (2010).

11. Rohringer, N. et al. Atomic inner-shell X-ray laser at 1.46 nanometres pumped by an X-ray free-electron laser. *Nature* **481,** 488–491 (2012).

12. Kanter, E. P. et al. Unveiling and driving hidden resonances with high-fluence, high-intensity X-ray pulses. *Phys. Rev. Lett.* **107,** 233001 (2011).

13. Weninger, C. et al. Stimulated electronic X-ray Raman scattering. *Phys. Rev. Lett.* **111,** 233902 (2013).

14. Tamasaku, K. Double core-hole creation by sequential attosecond photoionization. *Phys. Rev. Lett.* **111,** 043001 (2013).

15. Tamasaku, K. et al. X-ray two-photon absorption competing against single and sequential multiphoton processes. *Nature Photon.* **8,** 313–316 (2014).

16. Shwartz, S. et al. X-ray second harmonic generation. *Phys. Rev. Lett.* **112,** 163901 (2014).

17. Eisenberger, P. & McCall, S. L. X-ray parametric conversion. *Phys. Rev. Lett.* **26,** 684–688 (1971).

18. Freund, I. & Levine, B. F. Parametric conversion of X rays. *Phys. Rev. Lett.* **23,** 854–857 (1969).

19. Brown, L. S. & Kibble, T.W. B. Interaction of intense laser beams with electrons. *Phys. Rev.* **133,** A705_A719 (1964).

20. Chen, S.-Y., Maksimchuk, A. & Umstadter, D. Experimental observation of relativistic nonlinear Thomson scattering. *Nature* **396,** 653_655 (1998).

21. Bula, C. et al. Observation of nonlinear effects in Compton scattering. *Phys. Rev. Lett.* **76,** 3116_3119 (1996).

22. Glover, T. E. et al. X-ray and optical wave mixing. *Nature* **488,** 603–608 (2012).

23. Huang, Z. & Kim, K.-J. Review of x-ray free-electron laser theory. *Phys. Rev. Spec. Top. Accel. Beams* **10,** 034801 (2007).

24. Sauter, F. Über das Verhalten eines Elektrons im homogenen elektrischen Feld nach der relativistischen Theorie Diracs. *Z. Phys.* **69,** 742–764 (1931).

25. Schwinger, J. On gauge invariance and vacuum polarization. *Phys. Rev.* **82,** 664–679 (1951).

26. Boutet, S. & Williams, G. J. The Coherent X-ray Imaging (CXI) instrument at the Linac Coherent Light Source (LCLS). *New J. Phys.* **12,** 035024 (2010).

27. Hubbell, J. H. & Seltzer, S. M. Tables of X-ray Mass Attenuation Coefficients and Mass Energy-Absorption Coefficients (version 1.4) (National Institute of Standards and Technology, 2004); http://physics.nist.gov/xaamdi

28. Herrmann, S. et al. CSPAD-140 k: A versatile detector for LCLS experiments. *Nucl. Instrum. Methods Phys. Res. A* **718,** 550–553 (2013).

29. Sarachik, E. S. & Schappert, G. T. Classical theory of the scattering of intense laser radiation by free electrons. *Phys. Rev. D* **1,** 2738–2753 (1970).

30. Klein, O. & Nishina, Y. Über die Streuung von Strahlung durch freie Elektronen nach der neuen relativistischen Quantendynamik von Dirac. *Z. Phys.* **52,** 853–868 (1929).

31. Hämäläinen, K. et al. High resolution Compton scattering study of Be. *Phys. Rev. B* **54,** 5453–5459 (1996).

32. Hopersky, A. N., Nadolinsky, A. M. & Novikov, S. A. X-ray-photon scattering by an excited atom. *Phys. Rev. A* **88,** 032704 (2013).

33. Hopersky, A. N., Nadolinsky, A. M., Novikov, S. A. & Yavna, V. A. X-ray-photon scattering by an excited and ionized atom. *Phys. Rev. A* **91,** 022708 (2015).

34. Henke, B.L., Gullikson, E.M. & Davis, J.C. X-ray interactions: Photoabsorption, scattering, transmission, and reflection at ED5030000 eV, Z D192. *At. Data Nucl. Data Tables* **54,** 181342 (1993).

35. Ratner, D. *et al.* Second and third harmonic measurements at the linac coherent light source. *Phys. Rev. Spec. Top. Accel. Beams* **14,** 060701 (2011).